Critical behavior of a smectic-*A* to nematic phase transition imbedded in a random network of voids

Sihai Qian,* Germano S. Iannacchione,† and Daniele Finotello
Department of Physics, Kent State University, Kent, Ohio 44240
(Received 13 August 1997)

We present the results of a systematic ac calorimetric study on the smectic-*A* to nematic (Sm-*A*–*N*) phase transition for the alkylcyanobiphenyl liquid crystals, 8CB and 9CB, imbedded in the randomly interconnected voids of Millipore cellulose membranes. The confining void size ranged from 5 to 0.025 μm, which, although large, introduces substantial changes compared to the bulk behavior. The heat capacity peak at the Sm-*A*–*N* transition temperature changes from sharp and prominent to broad and small with increased confinement. Concomitant with the heat capacity peak shape change, critical behavior analysis reveals that the random confinement drives the heat capacity critical exponent from its bulk value towards zero, approaching the three-dimensional *XY* universality class value prediction of -0.007. This change in the critical exponent is liquid-crystal material and voids size dependent, and is equivalent to what occurs with increasing nematic range that weakens the coupling between smectic and nematic order parameters. The Millipore confinement does not alter the nematic range; it is the randomness it introduces that changes the nature of the coupling. In addition, but in a manner not fully consistent with finite size effects, transition temperatures are shifted down from bulk and the transition enthalpy is suppressed. Supporting results are found in a study of binary mixtures of 9CB and 10CB. [S1063-651X(98)02504-5]

PACS number(s): 64.70.Md, 61.30.−v, 65.20.+w

INTRODUCTION

Due to the technological relevance of liquid crystals in the rapidly growing display industry, and the highly influential role that surfaces exert on the behavior of fundamental liquid-crystal properties, considerable attention has been recently devoted to the study of confined liquid-crystal systems. Liquid crystals, particularly cyanobiphenyls, have been studied while imbedded in a variety of porous solid substrates. These include the random interconnected network of pores of Aerogel [1] and Vycor glasses [2], and the parallel cylindrical pores of aluminum oxide Anopore [3] and polycarbonate Nuclepore [4].

Partly because of their added complexity and less viable application possibilities, fewer research efforts have dealt with confinement effects on smectics than on nematics. Besides orientational order, the smectic-*A* phase possesses one-dimensional positional or translational order. This translational order is much more sensitive than the orientational order to the curvature of the host porous media [3,5]. As for nematics, the smectic-*A* phase deforms depending on the elastic properties, external field, surface condition (curvature and roughness) or nematic history. Thus past research dealing with a confined smectic-*A* to nematic (Sm-*A*–*N*) transition focused on molecular structural configurations. For instance, it was shown by Cladis [6] that smectic fluctuations reduce the nematic bend and twist deformation. Chevron and radial configurations of smectic layers [7] and discrete layering growth [8] are possible depending on surface preparation and confinement conditions.

The bulk Sm-*A*–*N* transition is believed to belong to the three-dimensional (3D) *XY* universality class characterized by a heat capacity critical exponent $\alpha = -0.007$ [9]. The critical exponent is influenced by the strength of the coupling between the nematic orientational order parameter and the order parameter for the one-dimensional layered structure of the smectic-*A* phase [10]. Depending on the nematic range (NR) ($\mathrm{NR} \equiv T_{N\text{-}I} - T_{\mathrm{Sm}\text{-}A\text{-}N}$) where $T_{\mathrm{Sm}\text{-}A\text{-}N}$ and $T_{N\text{-}I}$ are the smectic-*A* to nematic and nematic to isotropic transition temperatures, the Sm-*A*–*N* transition may change from first order to second order. The temperature at which such change occurs is called the tricritical point. As a function of the coupling between the two order parameters, stronger for a narrow nematic range material (or larger McMillan ratio defined as $T_{\mathrm{Sm}\text{-}A\text{-}N}/T_{N\text{-}I}$), the Sm-*A*–*N* transition is driven away from the 3D-*XY* behavior towards tricritical behavior, or, to some intermediate value between them. Critical exponents obtained in the latter case are called ''effective'' or ''crossover'' exponents.

The liquid-crystal materials used in this work, *n*CB with *n* either 8 or 9, where *n* is the number of carbons in the alkyl chain, have been an excellent example to appreciate the critical behavior evolution as a function of nematic range [11]. When $n = 7.56$ (a mixture of 56% 8CB in 7CB) and a 15 K nematic range, the heat capacity critical exponent α is -0.03, in agreement with the 3D-*XY* model prediction. When $n = 9$, the nematic range decreases to 1.9 K, and a tricritical $\alpha = 0.5$ is obtained. In between, when $n = 8$, the nematic range is 7.1 K, α is about 0.3, a nonuniversal effective exponent. Similar results have also been obtained in thiosulfate, *n*S5 for short [12,13], and in $DB_8ONO_2 + DB_{10}ONO_2$ binary mixtures [14], where again

*Present address: Physical Optics Co., 20600 Gramercy Place, Bldg. 100, Torrance, CA 90501.
†Present address: Dept. of Chemistry, M1T, Cambridge, MA 02139.

the critical exponent changes from the 3D-XY to the tricritical value depending on the width of the nematic range.

To summarize the bulk Sm-$A-N$ transition, the results suggest that 3D-XY behavior occurs for materials with large nematic ranges, tricritical behavior for short nematic ranges, while a crossover effective value is found for intermediate nematic ranges. In terms of the McMillan ratio, $T_{N-\text{Sm-}A}/T_{N\text{-}I}$, the heat capacity behavior is in good agreement with 3D-XY predictions for all samples where the ratio is $\leqslant 0.93$; for short nematic range or $T_{\text{Sm-}A-N}/T_{N\text{-}I} \geqslant 0.93$, the expected cross-over to tricritical behavior is seen. See further details in the review by Garland and Nounesis [9].

Under confinement, that is, liquid crystals imbedded in geometries more restrictive than bulk, a systematic investigation at the Sm-$A-N$, N-I, and Sm-$A-I$ (smectic-A to isotropic) phase transitions was undertaken by Finotello and co-workers [2–4]. The confinement was achieved with the surface-treated and untreated cylindrical pores of Anopore membranes as a function of nCB liquid-crystal material. Clark, Garland, and collaborators [1] also investigated the Sm-$A-N$ transition of 8CB but confined to the random network of interconnected pores of silica Aerogel and as a function of pore size. Common features revealed by these specific heat measurements are that, when contrasted to bulk (i) the transition temperature $T_{\text{Sm-}A-N}$ shifts downward; (ii) the Sm-$A-N$ specific heat peak is small, broad, and rounded; and (iii) results are not fully consistent with finite size effect expectations.

The usually considerable suppression of the specific heat peak at the confined Sm-$A-N$ transition has prevented previous studies from extracting the heat capacity critical exponent α and its dependence on the confining size. In this paper, we address the effects that confinement to Millipore filters introduces at the smectic-A to nematic transition for two members of the nCB series, 8CB and 9CB. Even though the transition specific heat peak is suppressed, it remains sharp enough that a reliable critical behavior analysis can be performed; critical exponents can thus be extracted and their dependence on void size established. These results are further supported by calorimetric studies with binary mixtures of 9CB with 10CB in 0.05 μm Millipore also included here. A shorter version of this work has already appeared in the literature [15]. Similar results where the heat capacity critical exponent is altered by a random confinement have also been reported in a recent calorimetry study at the 8CB Sm-$A-N$ transition perturbed by the presence of submicrometer size silica spheres (or Aerosil) [16]. Finally, although some features related to the higher-temperature N-I transition will be presented, the complete discussion of several interesting phenomena occurring at the N-I transition is deferred to a different paper, here, we concentrate mostly on aspects pertaining to the Sm-$A-N$ transition.

EXPERIMENTAL RESULTS

Our motivation comes from the existing studies of bulk and confined phase transitions in cyanobiphenyl liquid crystals. In particular, 8CB has been studied extensively in bulk form [17–19], and confined to several substrates that include Anopore [3], silica Aerogel [1,20,21], Aerosil [16], Vycor [2,22], and Vycor-like porous glass [23,24]. As stated earlier, for bulk 8CB, a nonuniversal behavior characterized by an ''effective'' Sm-$A-N$ heat capacity critical exponent α ranging between 0.26 [3] and 0.31 [8,17–19] is found. The 9CB Sm-$A-N$ transition is located at the tricritical point with $\alpha \approx 0.5$ [11], a Gaussian tricritical value.

TABLE I. Characteristics of the Millipore samples. The nominal void size, likely the shortest length scale of the membranes, is as quoted by the manufacturer. The SEM results report our analysis of the photographs. The x-ray column represents the smectic correlation length shown in Fig. 1 $\langle V_A \rangle$ is the average of the nominal, SEM, and x-ray values while the porosity was estimated from the SEM photographs. NA means not available.

Sample	Nominal (μm)	SEM (μm)	X-ray (μm)	$\langle V_A \rangle$ (μm)	Porosity %
5000M	5	$\sim$7.5	NA	6.25	NA
800M	0.8	$\sim$3	NA	1.9	72
220M	0.22	$\sim$0.7	0.315	0.41	69
100M	0.1	0.3	0.165	0.19	56
50M	0.05	0.3	0.12	0.16	62
25M	0.025	0.2	0.09	0.11	51

Experimental samples and technique

For completeness and a more reliable data comparison, the same batch of bulk 8CB, purchased from BDH [25], was used for all bulk and confined samples. The porous host substrate, Millipore membranes, is made from biologically pure inert mixtures of cellulose acetate and cellulose nitrate [26]. To visualize these membranes, Millipore resemble the type of random network that is achieved in liquid-crystal–polymer mixtures [22]. This morphology is thus distinct from that of a porous glass (e.g., Vycor) where the liquid crystal is confined to well-defined solid walls.

The Millipore membranes, of thickness ranging between 90 and 170 μm depending on void size, are available in several void sizes, with six different void sizes used in the 8CB study. The manufacturer's quoted (nominal) void sizes employed were 0.025, 0.05, 0.1, 0.22, 0.8, and 5 μm. However, as determined from our scanning electron microscopy (SEM) studies, the actual average void sizes range from 0.2 to 7.5 μm, with a wide void size distribution for each filter. Therefore we suspect that the manufacturer size refers to the smallest voids in each membrane. The void size characteristics are given in Table I. Despite the void size magnitude ambiguity, a precise knowledge is not crucial to the results described here.

Because of the randomness of the material and uncertainties on the void size, we also performed some characterization measurements with liquid crystals imbedded in the membranes. First, for 8CB in Millipore, from small angle neutron scattering (SANS) that was performed in collaboration with Sokol at Argonne National Laboratories in the 50M sample voids, we directly proved the presence of smectic layers [27]. These were found to have a bulklike spacing of roughly 31.4 Å. In addition, the length at which the smectic correlation length saturates, $\xi_{\parallel \text{sat}}$, was determined from x-ray measurements. These results obtained by Clark and students at Brookhaven [28] are shown in Fig. 1 and are listed in

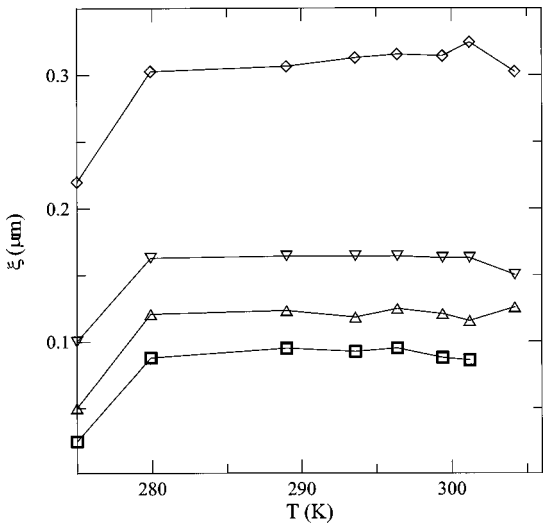

FIG. 1. Smectic correlation length as a function of temperature. Note the nearly constant correlation length value that is larger than the nominal void size. The nominal size is indicated by the symbols at the vertical axis. This study was performed by Clark and coworkers.

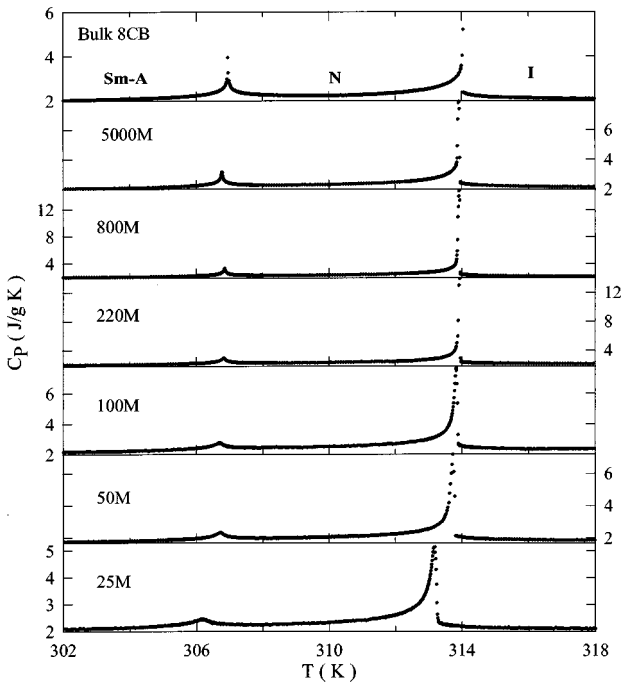

FIG. 2. Specific heat of bulk and Millipore confined 8CB samples as a function of temperature showing the high-temperature isotropic (I), the intermediate-temperature nematic (N), and the low-temperature smectic-A (Sm-A) phases. For sample legends see Table I.

Table I. Below the transition, and over a wide temperature range, $\xi_{\|}$ is temperature independent, on average saturating at 0.315, 0.165, 0.12, and 0.09 μm for nominal void sizes corresponding to 0.22, 0.1, 0.05, and 0.025 μm, respectively. The saturated correlation length values are reasonably close to the void size estimated from the SEM photographs. In short, the nominal size is probably the smallest size in the system; the photograph analysis performed in a small window of the sample might be inclined to select a larger size; the x-ray work is sensitive to the mean smectic domain size; thus we have chosen to average these values and use them ($\langle\langle V_A\rangle$ in Table I is the average void size) hereafter.

The heat capacity was measured by means of a high-resolution ac calorimetry technique [29] with samples containing approximately 2–4.5 mg of liquid-crystal material imbedded in a single Millipore piece cut to a square, 6 mm on a side. Measurements take place under near equilibrium conditions since very small temperature oscillations about a precisely determined average temperature are applied to the sample. The amplitude of the resulting temperature oscillations, $T_{\rm ac}$, is inversely proportional to the heat capacity of the sample, C, and can be expressed as

$$T_{\rm ac}=\{Q_0/2\omega C\}\{1+(\omega\tau_e)^{-2}+(\omega\tau_i)^2\}^{-1/2}, \qquad (1)$$

where the thermal relaxation times are defined as $\tau_e = C/K_b$ (external) and $\tau_1^2=\tau_\theta^2+\tau_h^2+\tau_s^2$ (internal). The individual relaxation times $\tau_\theta=C_\theta/K_\theta$, $\tau_h=C_h/K_h$, and $\tau_s = C_S/K_S$ correspond to the thermometer, heater, and sample, respectively. The C's and K's represent the individual heat capacity and thermal conductivity. The internal relaxation time constant is the time required for the entire assembly to reach equilibrium with the applied heat while the external relaxation time constant is the time required for equilibration with the surrounding thermal bath.

The calorimeter has an internal time constant between 1 and 2 s (typically a 0.79 Hz high-frequency roll off) and an external time constant of $\sim$30–40 s (usually a 0.032 Hz low-frequency roll off). The addendum heat capacity, which is 31 mJ/K at 316 K, increases linearly at a rate of 0.103 mJ/K^2. The applied voltage frequency was typically 55 mHz and the amplitude of the induced temperature oscillations was kept at 2 mK peak to peak. Data are taken every 10 mK, and after a wait of 7 min at the new temperature, it is averaged for 8 to 10 min. The temperature regulation is better than 80 μK.

Specific heat of 8CB in Millipore

The specific heat dependence on temperature for bulk and for the confined samples is shown in Fig. 2. This plot illustrates a wide temperature range enclosing the isotropic, nematic, and smectic-A phases. The Sm-A–N and N-I transition temperatures for bulk 8CB are 306.95 and 314.04 K, respectively. The confined $T_{\text{Sm-}A-N}$ and T_{N-I} are shifted below the respective bulk transitions. The confined nematic range hardly changes compared to bulk being constant at 7.06 $\pm$0.07 K.

First, not according to finite size effect expectations, a well-defined trend in $T_{\text{Sm-}A-N}-T_{\text{Sm-}A-N}$ (bulk) vs void size does not appear to be present in Millipore. This is in contrast to 8CB confined to silica Aerogel [1] where this transition shifts progressively downward with decreasing pore size. The difference in $T_{\text{Sm-}A-N}$ (confined) dependence on size between these two host materials is that, besides their different morphology, in Aerogel, the smaller pore size may play a more important role in shifting the transition by as many as 3 K. The Millipore voids are quite large and its fibers either behave like an impurity in the liquid-crystal material, or play a role equivalent to that of surface disorder. It is also conceivable that since Millipore are produced from mixtures of cellulose, the surface–liquid-crystal interaction changes with

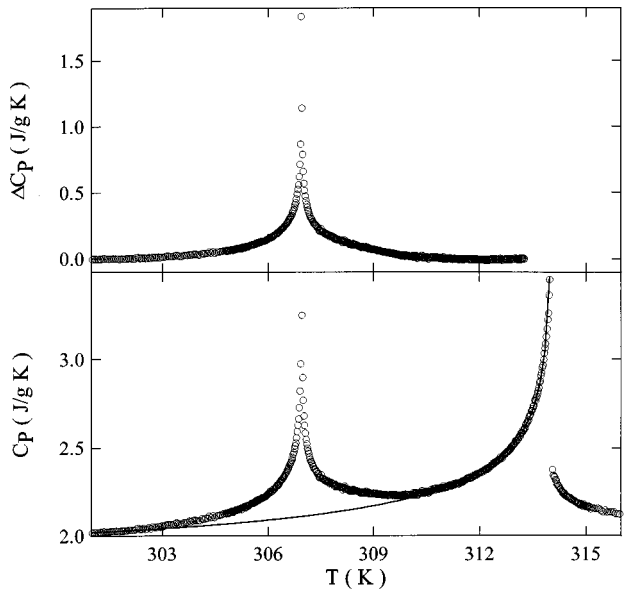

FIG. 3. Typical extraction of the Sm-$A-N$ excess specific heat peak (upper panel) after subtraction of the low-temperature wing (solid line) of the N-I transition from the total specific heat (bottom panel). Data shown correspond to bulk 8CB.

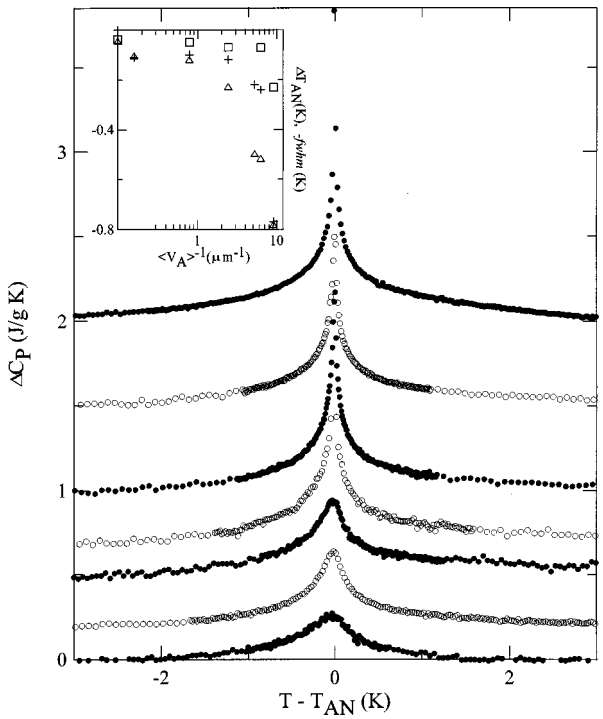

FIG. 4. Excess specific heat for bulk and Millipore confined 8CB near the transition temperature $T_{\text{Sm-}A-N}$. From top to bottom, data are for bulk, 5000M, 800M, 220M, 100M, 50M, and 25M samples. Data have been shifted for clarity. Inset: Transition shift (+8CB) and full width at half maximum (△, 8CB and □, 9CB) dependence on the inverse average void size given in Table I.

void size. Except for the smallest void size (25M) where the shift is 0.8 K, the change in transition temperature ranges from 110 to 240 mK when $\langle V_A \rangle$ changes by nearly two orders of magnitude. However, as seen later, combining the Millipore with the Aerogel results yields a reasonable overall-decreasing trend with size.

To extract the transition peak, as required for the critical behavior analysis that follows, the low-temperature wing of the N-I transition is subtracted from the total measurement. This is exemplified with the bulk 8CB results. Data close to $T_{N\text{-}I}$ and on the lower-temperature side of the N-I transition together with data far below $T_{\text{Sm-}A-N}$ are fitted to a power law function; this is indicated by the solid line in the bottom panel of Fig. 3. The Sm-$A-N$ transition peak ΔC_P so extracted is shown in the top panel of Fig. 3. This procedure is consistently repeated for each confined sample and the Sm-$A-N$ ΔC_P's for bulk and Millipore confined 8CB are plotted in Fig. 4 as a function of temperature shift $T-T_{\text{Sm-}A-N}$.

In the largest Millipore voids, the transition peaks retain their sharpness; with decreasing void size, they become broad, round, and suppressed. Such effect can be partly quantified by the peak's full width at half maximum (FWHM). The FWHM increases from 103 ± 13 to 780 ± 86 mK while $\langle V_A \rangle$ decreases from 6.25 to 0.11 μm. A more rapid increase takes place for void sizes less than 0.4 μm as indicated in the inset to Fig. 4. The effect of Millipore can also be quantified by the transition enthalpies, calculated from $\Delta H_{\text{Sm-}A-N}=\int \Delta C_P dT$ over the temperature interval $T_{\text{Sm-}A-N}\pm3$ K range; $\Delta H_{\text{Sm-}A-N}$ decreases with decreasing void size. The relative enthalpy change with respect to the bulk value as a function of the average void size is plotted in the top panel of Fig. 5. Again, below a 0.4 μm void size (220M sample) there is a steeper dependence in the enthalpy. The characteristic features of the 8CB Sm-$A-N$ transition are summarized in Table II.

Following Rappaport *et al.* [30], we test for a finite size effect influence in the transition enthalpy by assuming that the confined behavior is like bulk's with the bulk specific heat peak limited in its growth and thus truncated at some length scale. Specifically, this is done by calculating ΔT from $\xi=\xi_0|\Delta T|^{-\nu_\parallel}$, where ξ_0 is 208 Å, $\nu_\parallel=0.67$ (see, for instance, references found in [1,9,30]), $\Delta T=T-T_{\text{Sm-}A-N}$, and substituting for ξ the nominal void size R. To obtain the largest enthalpy suppression, we choose R since it is the smallest length in the system. Despite our choice, shown by the dashed line in Fig. 5, this bulklike ''constrained'' enthalpy completely misses the experimental results. The reduction of enthalpy is likely related to the existence of a liquid-crystal layer at the Millipore fibers, which is incapable of forming a smectic-A phase. Such molecules are orientationally frozen in a state of low order; a change to a smectic would energetically be prohibitive due to elastic deformations [3,16].

Comparing Millipore with Aerogel yields a clearer void (pore) size dependence of some of the confined parameters. In Fig. 5 we also plot the transition temperature shift and the magnitude of the specific heat $\Delta C_{P\,\max}$ (ΔC_P evaluated at $T_{\text{Sm-}A-N}$) as a function of L^{-1}. In this plot, L represents either the mean pore size in Aerogel, or the saturated smectic correlation length in Millipore. Taking all data together, there is a clearly defined decreasing trend in both quantities for smaller L, with the specific heat maximum rapidly becoming quite small. Such a rapid decrease in amplitude with increased confinement is to be blamed for the lack of prior critical behavior analysis. Although no error bars are shown,

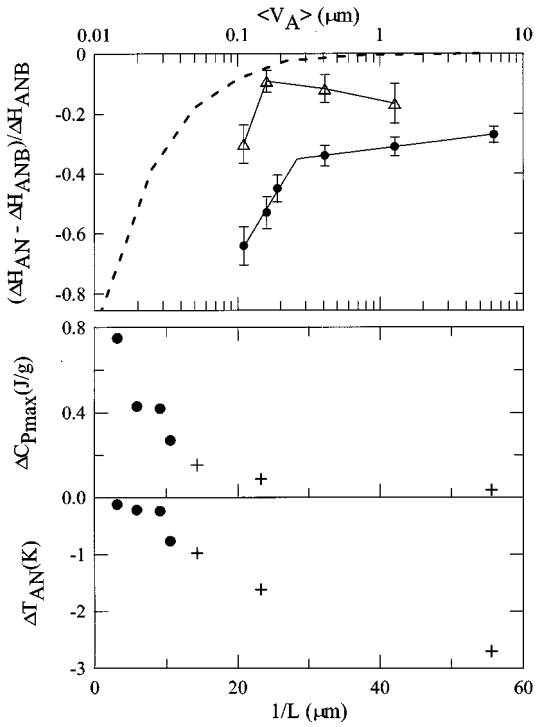

FIG. 5. Top panel: Decrease of the relative Sm-$A-N$ transition enthalpy compared to the bulk value as a function of V_A for (●) 8CB and (△) 9CB in Millipore. The dashed line is a finite size expectation for a bulklike 8CB peak truncated at the nominal size (see text). Center panel: Specific heat maximum at $T_{\text{Sm-}A-N}$ as a function of inverse length for 8CB in Millipore (●) and in Aerogel (+). Bottom panel: Transition shift as a function of inverse length L for 8CB in Millipore and in Aerogel. L is either the smectic correlation (Millipore) or the average pore chord size (Aerogel).

TABLE II. Characteristics of the bulk and Millipore confined Sm-$A-N$ transition. The errors quoted are the statistical uncertainties. See text for the temperature range of the enthalpy calculation.

Sample		$T_{\text{Sm-}A-N}$ (K)	$\Delta H_{\text{Sm=}A-N}$ (J/g)	FWHM (mK)	NR (K)	$\Delta C_{P\,\max}$ (J/g)
8CB	bulk	306.95	0.94±0.05	44±10	7.09	1.83
	5000*M*	306.84	0.69±0.05	103±13	7.08	1
	800*M*	306.85	0.65±0.05	119±13	7.09	1.17
	220*M*	306.83	0.62±0.05	227±23	7.11	0.75
	100*M*	306.73	0.56±0.05	497±37	7.10	0.43
	50*M*	306.71	0.44±0.05	516±31	7.03	0.43
	25*M*	306.18	0.34±0.05	781±86	6.99	0.27
9CB	bulk	321.21	1.26±0.09	38±5	1.87	7.84
	800*M*	320.76	1.05±0.05	50±6	1.93	5.03
	220*M*	320.53	1.11±0.05	69±7	1.90	3.8
	50*M*	320.98	1.14±0.05	71±7	1.87	4.15
	25*M*	320.81	0.88±0.05	231±10	1.76	1.28
9.05CB	bulk	321.43	1.47±0.09	50±6	1.63	8.65
	50*M*	320.36	1.12±0.09	100±12	1.72	4.01
9.11CB	bulk	321.57	1.32±0.09	55±6	1.30	7.65
	50*M*	320.88	0.90±0.09	90±10	1.32	3.52

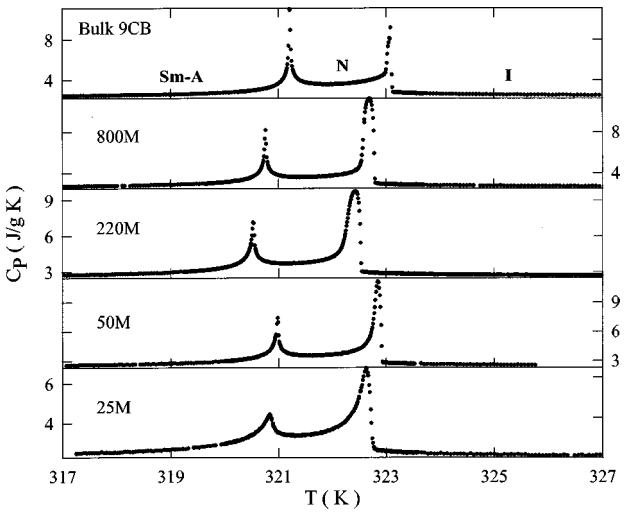

FIG. 6. Specific heat of bulk and Millipore confined 9CB as a function of temperature including isotropic, nematic, and smectic-*A* phases.

the accuracy and density of data are not enough to determine an accurate functional dependence of α on the confining size L.

In short, when viewed independently of other host materials, for all Millipore confined 8CB (and as discussed below 9CB) samples, $T_{\text{Sm-}A-N}$ is shifted down with respect to bulk but lacking a regular dependence on decreasing void size. This suggests that the surface condition of the Millipore filters is void size independent. For host materials with well-defined solid surfaces [1–5], surface-induced ordering and disordering compete to determine the transition temperature. Introducing bulk deformations due to the arrangement of surfaces that depress transition temperatures [2,32–34] manifests disordering. The surface ordering effects are like those of an external magnetic field on a spin system, and increase the transition temperature [35]. The composition of Millipore filters, a mixture of cellulose acetate and cellulose nitrate, makes the surface more likely to have a random roughness independent of void size. As seen in our NMR studies in Millipore [36], the ordering effects that are present are weaker (~by a factor of 2) than those in the other porous substrates. In general, in all confined studies to date, there has been no dominant mechanism that is solely responsible for shifting the transition temperature, rather, the shift probably depends on the combination of several effects: finite size effects, competition of surface order or disorder, elastic distortions, and random field effect [1–3,16].

Specific heat of 9CB in Millipore

The Sm-$A-N$ transition in bulk and Millipore confined 9CB was studied on the same calorimeter employing four sizes: 800*M*, 220*M*, 50*M*, and 25*M*. Plotted in Fig. 6 are the specific heat results over a wide temperature range that includes the isotropic, nematic, and smectic-*A* phases. The transition temperatures of bulk 9CB are $T_{\text{Sm-}A-N} = 321.21$ K and $T_{N-I} = 323.08$ K while both confined transition temperatures are shifted below bulk; the nematic range is basically constant at 1.86±0.1 K. $T_{\text{Sm-}A-N}$ decreases from bulk when confined to the 800*M* sample; it is further depressed in the 220*M* voids. With increased confinement to

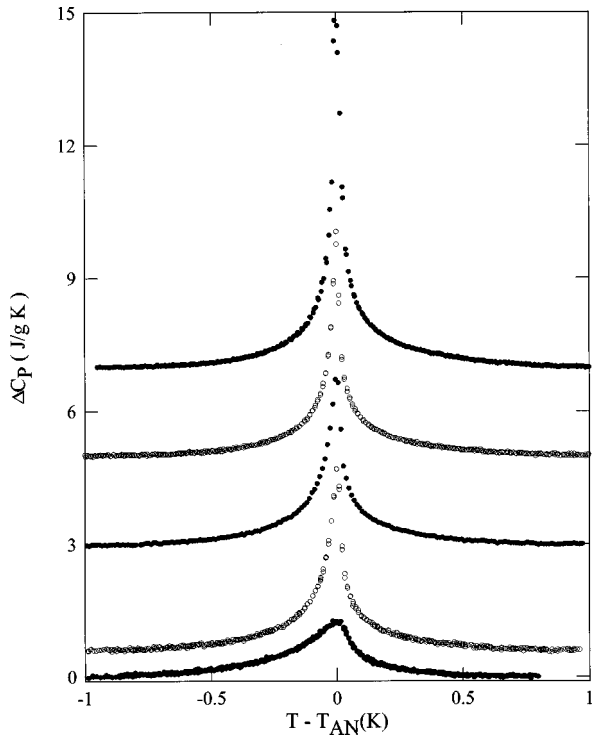

FIG. 7. Excess specific heat of bulk and Millipore confined 9CB. Data have been shifted for clarity. From top to bottom, data are for bulk, 800*M*, 220*M*, 50*M*, and 25*M* samples.

50*M* Millipore, $T_{\text{Sm-}A-N}$ is below bulk's but higher than in the larger Millipore sizes. We do not understand this behavior, but certainly, more than finite size effects is suggestive of either impurity or surface-disorder type of effects, in addition to possible changes in the liquid crystals anchoring energy in the Millipore samples. A summary of the 9CB specific heat peak characteristics is included in Table II.

The same procedure described earlier is employed to extract the Sm-*A* excess specific heat ΔC_P for 9CB shown in Fig. 7 as a function of temperature. More so than in 8CB, the 9CB confined transition peak retains its bulklike divergence in all cases except for the smallest void size sample, 25*M*. There, the peak is broad and round. The 9CB specific heat evaluated at the transition temperature, Table II, also decreases with increased confinement. Calculation of the FWHM reveals that for the largest void size samples the width of the transition peak increases marginally with decreasing void size. Again, a drastic increase is found but now occurring at a smaller void size than for 8CB: between the 50*M* and 25*M* sample sizes. See the inset to Fig. 4. The 9CB Sm-$A-N$ confined transition enthalpies exhibit a weaker void size dependence than in 8CB. Determined over the narrower temperature range $T_{\text{Sm-}A-N} \pm 1$ K due to 9CB's nematic range, the confined $\Delta H_{\text{Sm-}A-N}$ (see Fig. 5), has an average value of 1.1 ± 0.06 J/g for the three largest Millipore samples, a 12% decrease from bulk but showing a slight increasing trend with decreasing void size. We do not believe that such apparent increase is significant, rather, it is a consequence of the narrow temperature window used which increases the error in the calculation. For the 25*M* sample there is an unmistakable 30% decrease from bulk to $\Delta H_{\text{Sm-}A-N} = 0.88 \pm 0.05$ J/g. The difference in the behavior

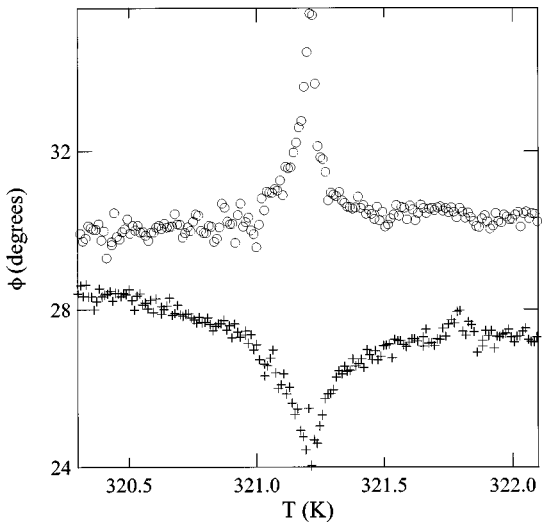

FIG. 8. Phase shift behavior near the smectic to nematic transition for bulk 9CB (+) and for 9CB confined to 220*M* Millipore (○).

of 8CB and 9CB within Millipore as a function of confining size appears to be related to their nematic range and consequently, the coupling strength between smectic and nematic order parameters.

Phase shift signature

In ac calorimetry measurements, in addition to the heat capacity, the phase shift is simultaneously acquired. The phase shift contains qualitative information on both the heat capacity and the thermal conductivity of the sample [29]. It is empirically found [1,3,29,31] that at a first order transition there is a peaklike signature in the phase shift; at a second order transition the signature at the transition temperature is a dip. Shown in Fig. 8, as expected from its second order character, bulk 9CB exhibits a dip in the phase shift at $T_{\text{Sm-}A-N}$. In contrast, for all Millipore confined samples, a peak in the phase shift replaces the dip. An example of the confined phase shift behavior is also illustrated in Fig. 8 for 9CB confined to the 220*M* sample. A change in phase shift alone cannot be taken as unambiguous evidence of a change in the order of the transition. Thus we simply interpret this as additional evidence that the confined behavior near the transition is distinct from bulk's.

Specific heat of 9CB doped with 10CB

For reasons that are connected to the critical behavior analysis described below, we also studied the Sm-$A-N$ transition after doping 9CB with a small amount of smectic 10CB (no nematic phase is present in 10CB). We studied two bulk mixtures as well as confined to the 0.05 μm nominal Millipore void size: 11.4%, and later, 4.8% of 10CB in 9CB, hereafter named 9.11CB and 9.05CB, mixtures that are presumably beyond the tricritical point (located at 8.96CB [9]). The excess specific heat dependence on temperature for these mixtures, extracted as before, is shown in Fig. 9. Note from this plot that away from the transition, the bulk and confined data overlay one another. Near the transition, and more obvious on the nematic side, the confined data lie be-

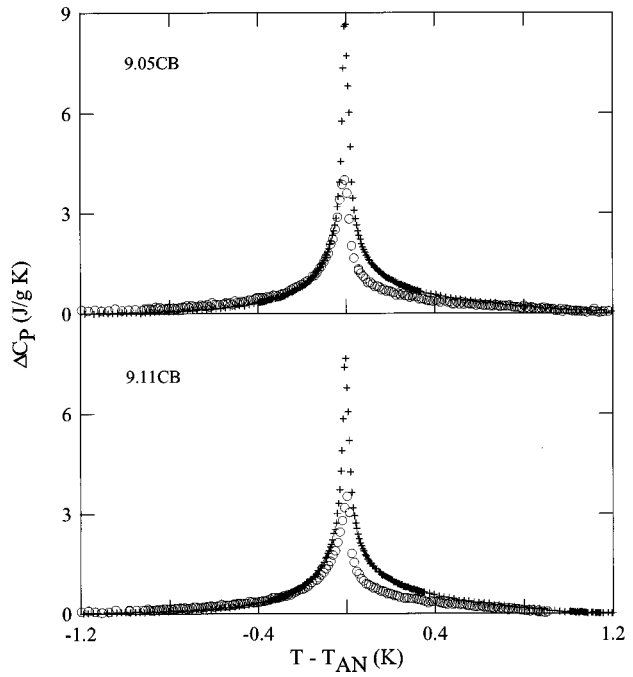

FIG. 9. Excess specific heat for bulk (+) and 50*M* Millipore (○) confined (9+10)CB mixtures.

low bulk. This probably reflects the difficulty in forming the smectic phase because of an orientationally frozen layer at the Millipore fibers.

As expected given the increase in smectic component, the bulk mixtures show a narrower (than pure 9CB) nematic range with increased 10CB concentration. For bulk 9.05CB, the transition temperatures are $T_{\text{Sm-}A-N}=321.43$ K and $T_{N\text{-}I}=323.06$ K yielding a 1.63 K nematic range, a 12.8% reduction from pure 9CB. For bulk 9.11CB, $T_{\text{Sm-}A-N}=321.57$ K and $T_{N\text{-}I}=322.87$ K, and the nematic range is 1.30 K, or, a $\sim$30% reduction from pure 9CB. Under the 50*M* Millipore confinement, the transition temperatures are lowered by nearly the same amount; the nematic range is unaltered. For 9.05CB, $T_{\text{Sm-}A-N}$ and $T_{N\text{-}I}$ decrease to 320.36 and 322.08 K, respectively; for 9.11CB, they shift to $T_{\text{Sm-}A-N}=320.88$ K and $T_{N\text{-}I}=322.20$ K. As with 9CB, the confined mixtures have a peak maximum which is suppressed by roughly 50% compared to its bulk value.

The mixtures transition enthalpy is calculated over different temperature ranges than for 9CB due to the varying nematic width. For 9.05CB, the range is $T_{\text{Sm-}A-N}\pm 1$ K resulting in $\Delta H_{\text{Sm-}A-N}=1.12\pm 0.09$ J/g for the Millipore sample, a 23.8% decrease from the bulk mixture value of 1.47 ± 0.09 J/g. For 9.11CB, calculated over the range $T_{\text{Sm-}A-N}\pm 0.8$ K, $\Delta H_{\text{Sm-}A-N}=0.90\pm 0.09$ J/g for the confined sample, a 31.8% deficit from the corresponding bulk value of 1.32 ± 0.09 J/g. These results are summarized in Table II.

Critical behavior

The sharp and prominent smectic-*A* to nematic transition peaks found in 8CB and 9CB confined to Millipore filters allow us to carry out a critical behavior analysis. This is determined by fitting the excess specific heat of 8CB (Fig. 4), 9CB (Fig. 7), or (9+10)CB mixtures (Fig. 9) to a power law function in the reduced temperature t:

$$\Delta C_P = B_C + Lt + (A_\pm/\alpha)|t|^{-\alpha}(1+D_\pm|t|^{1/2}),$$

$$t=(T-T_C)/T_C. \quad (2)$$

The correction-to-scaling terms $D_\pm|t|^{1/2}$ [3,9,15,16,37,38] were needed (specifically for 9CB) since fits without it required drastically different values of the heat capacity amplitude, and, of the critical exponent above and below the Sm-$A-N$ transition. The exponent for the correction-to-scaling term is set equal to $\frac{1}{2}$ essentially the XY value of 0.524 [9,39]. It is a reasonable practice to include this term to describe the influence of the nearby N-I transition on the Sm-$A-N$ transition. The $\pm$ subscripts indicate parameters evaluated above and below the transition temperature. The constant B_C and the linear term Lt are introduced to account for any remnant background. The factor $A_\pm/\alpha$, rather than $A_\pm$ alone, allows α to continuously vary about zero. Typically, 300 data points on either side of T_C are simultaneously fitted using a standard nonlinear least-squares fitting method [40]. Range shrinking techniques were employed to test the stability of the resulting parameters and the final values are given in Table III.

The heat capacity exponent for the bulk 8CB Sm-$A-N$ transition is $\alpha=0.28\pm 0.02$, with an amplitude ratio $A_-/A_+=1.09\pm 0.05$, in good agreement with literature values [17–19]. In Fig. 10, top panel, we show $\log_{10}\{|(\Delta C_p - B_C - Lt)/(1+D_\pm|t|^{1/2})|\}$ vs $\log_{10}\{|(T-T_C)/T_C|\}$, which, from Eq. (2), yields two straight lines of slope $-\alpha$, for the data above and below T_C. The separation between the parallel lines is a measure of how different from unity is the amplitude ratio and consequently, the symmetry of the peak. To emphasize the quality of the fits, data points closer to T_C are replotted in the bottom panel using the magnified temperature upper x axis.

From these results it is evident that the specific heat exponent α tends to zero with decreasing void size. In the 5000*M* and 800*M* samples, α decreases to 0.18. Although representing a 35% reduction from the bulk value, it can still be considered an effective exponent. With increased confinement, i.e., decreasing void size, α tends towards zero, settling at a constant value 0.03 for void sizes smaller than 0.4 μm (220*M* sample). No negative α was obtained from these fits although an amplitude ratio $A_-/A_+<1$ was sometimes obtained during the range shrinking fit process. The ratio A_-/A_+ is near unity for every sample. Forcing α for the low-temperature (α_-) and high-temperature sides (α_+) to be the same, and a ratio $A_-/A_+=1$ indicates a highly symmetric peak. A few selected fits for Millipore confined 8CB are shown in Fig. 11.

The correction-to-scaling term $D_+|t|^{1/2}$ is small for bulk or confined 8CB samples. It has a magnitude of 0.2, 0.3, 0.4, 0.2, 0.05, 0.05, and 0.04, respectively, at $|t|=0.005$ for bulk and confined samples (with decreasing void size), compared with the dominating unity term [see Eq. (2)]. Previous determinations of the 8CB bulk exponent and amplitude ratio were obtained by fitting the data without including the correction-to-scaling term [19]. It is not surprising to obtain a small value for the correction-to-scaling term here in light of the ''wide'' 8CB nematic range. Interestingly, the contribution of the correction-to-scaling term becomes practically negligible below the 220*M* sample size. This could be taken

TABLE III. Least-squares parameter values from fits to the Sm-$A-N$ transition for 8 CB, 9 CB, and (9+10)CB mixtures. χ^2/N is the average accumulated squared deviation while t_m is the average of $t_{\min}(+)$ and $t_{\min}(-)$.

Sample	T_C (K)	α	A_-/A_+	D_-/D_+	B_C (J/g K)	L (J/g K)	χ^2/N (10^{-4})	$t_m\times10^{-4}$
8CB bulk	306.95	0.28±0.02	1.09±0.05	0.79±0.11	−0.21±0.08	−0.8±0.66	0.224	0.63
5000*M*	306.77	0.17±0.01	1.07±0.05	0.61±0.08	−0.86±0.09	−1.0±0.87	0.296	0.42
800*M*	306.85	0.18±0.01	1.10±0.05	0.53±0.07	−1.02±0.09	−3.74±1.09	0.509	0.51
220*M*	306.83	0.077±0.004	1.06±0.05	0.38±0.05	−2.690.14	−8.06±3.36	1.35	1.01
100*M*	306.72	0.029±0.002	1.04±0.05	0.18±0.03	−3.81±0.1	−3.95±3.02	1.24	1.26
50*M*	306.75	0.020±0.001	1.02±0.05	0.30±0.05	−6.83±0.12	−7.54±2.73	0.325	1.69
25*M*	306.22	0.036±0.004	1.05±0.05	−0.035±0.005	−2.12±0.11	−1.5±4.34	0.864	2.53
9CB bulk	321.22	0.52±0.02	1.32±0.05	2.82±0.25	0	−33±4.3	1.16	1.18
800*M*	320.76	0.51±0.02	1.56±0.05	0.99±0.09	1.14±0.14	−32.3±2.9	2.16	0.5
220*M*	320.54	0.37±0.02	1.65±0.05	0.16±0.02	−1.73±0.16	−55.1±9.6	2.0	0.66
50*M*	320.99	0.36±0.02	1.53±0.05	0.31±0.03	−2.15±0.18	−45.0±12.2	4.34	0.67
25*M*	320.86	0.037±0.002	1.09±0.05	−0.22±0.02	−9.25±0.43	−94.2±22.3	2.89	1.24
9.05CB bulk	321.43	0.51±0.01	1.23±0.04	0.86±0.21	18.6±1.3	−54.6±2.4	2.22	0.94
50*M*	320.36	0.50±0.01	2.3±0.08	0.46±0.27	6.5±2.11	−45.9±3.3	7.35	0.66
9.11CB bulk	321.57	0.50±0.01	1.44±0.02	0.72±0.16	22.2±3.2	−104±11	4.24	0.51
50*M*	320.88	0.49±0.01	2.51±0.17	0.41±0.1	11.2±1.4	−54±7.8	3.69	1.16

as an additional indication of a decoupling between the nematic and smectic order parameters.

Fits to Eq. (2) for the 9CB Sm-$A-N$ transition data are also performed following the same procedure employed for 8CB. The heat capacity exponent α and the amplitude ratio A_-/A_+ for bulk 9CB are 0.52 ± 0.01 and 1.32 ± 0.05, respectively, again in good agreement with published results [11,19,41]. In Fig. 12 we present the fits to Eq. (2) for bulk and the 800*M*, 220*M*, 50*M*, and 25*M* Millipore 9CB samples. For comparison, the 9CB bulk slope ($\alpha=0.52$) is included as a dashed line in each panel showing the confined data. The magnitude of the correction-to-scaling term

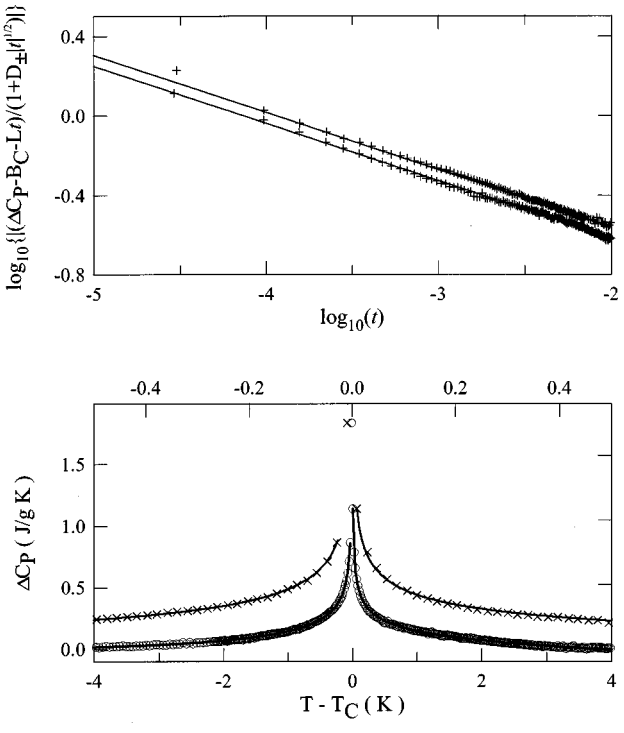

FIG. 10. Top panel: Fit to Eq. (2) for bulk 8CB. The solid lines are guides to the eye. As plotted, the slope yields the critical exponent α. Bottom panel: Bulk excess specific heat (○) as a function of separation from T_C. The same data are shown over a narrower temperature window using the upper x axis. The solid line is the fit to Eq. (2) using values of the parameters $B_C, L, \alpha, D_\pm, A_\pm$, obtained by fitting the data over the widest temperature range.

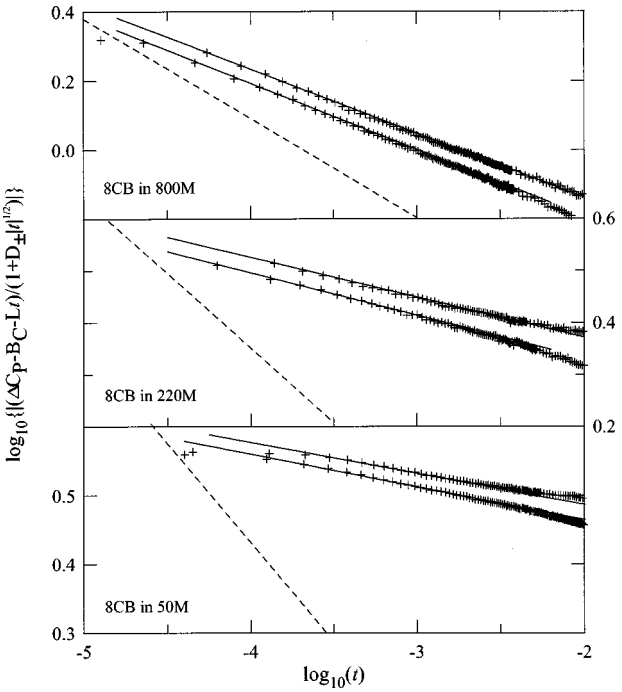

FIG. 11. Logarithmic plots for three different 8CB in Millipore samples. Notice the increasing difference in slope α with increased confinement as compared to bulk (dashed lines). Panels use different vertical scales for better data clarity.

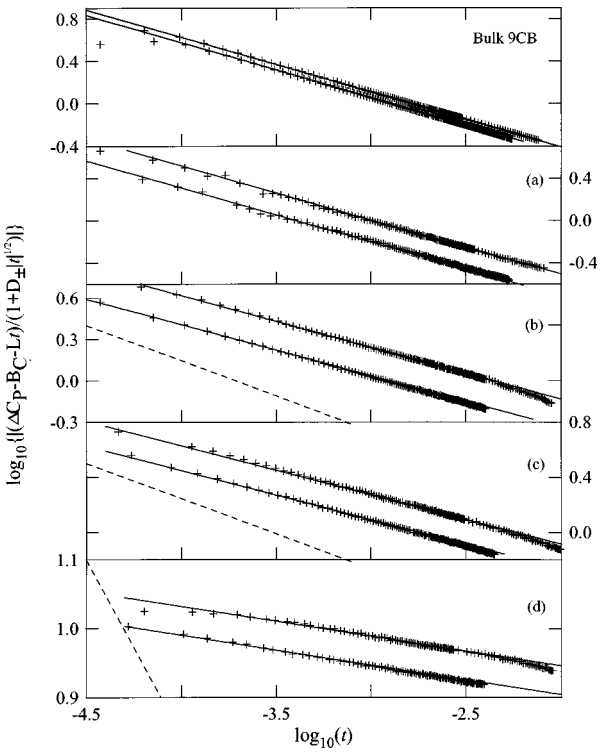

FIG. 12. Logarithmic plots for bulk and Millipore confined 9CB: (a) 800*M*, (b) 220*M*, (c) 50*M*, and (d) 25*M* samples. When the bulk slope α is different from the confined one, it is also shown by the dashed lines. The largest slope difference is evident in (d). Solid lines through the data are guides to the eye. Different vertical scales are used for better data visualization.

$D_+|t|^{1/2}$ at $|t|=0.003$ for 9CB is 5.6, 3.4, 1.8, 1.9, and 0.1 for bulk and decreasing Millipore void size, respectively. These values are considerably larger than those found for 8CB, reflecting the more important *N*-*I* influence on the 9CB Sm-*A*–*N* transition. Again, as for 8CB, such contribution drops dramatically for sizes below the 50*M* sample size.

A bulklike tricritical specific heat exponent is obtained for the 800*M* sample, $\alpha\approx 0.5$. For the 220*M* and 50*M* samples, α decreases to ~ 0.36, a 27% reduction from the bulk value, representing a crossover effective exponent. Finally, for the smallest void size (25*M*), a more drastic change takes place and a near zero α is obtained.

The changes in critical exponent with decreasing void size are related to how the random confinement alters the coupling between smectic and nematic order parameters. Increasing the coupling between order parameters can experimentally test this. We accomplished it by doping 9CB with small amounts of nematicless 10CB. In this way, the nematic width is decreased and consequently, the coupling enhanced. In addition, since the pure and mixture confined peaks are suppressed by almost the same amount, a comparison of the critical exponents is particularly meaningful.

The two liquid-crystal mixtures, whose excess specific heat was shown in Fig. 9, were also fitted to Eq. (2). The results of these fits for the bulk mixtures are presented in Fig. 13 and the critical behavior of both bulk mixtures is identical to that of the pure 9CB with $\alpha\sim 0.5$. The amplitude ratio A_-/A_+ is 1.23 ± 0.04 for 9.05CB and 1.44 ± 0.02 for 9.11CB respectively, not unlike the pure 9CB result of 1.32

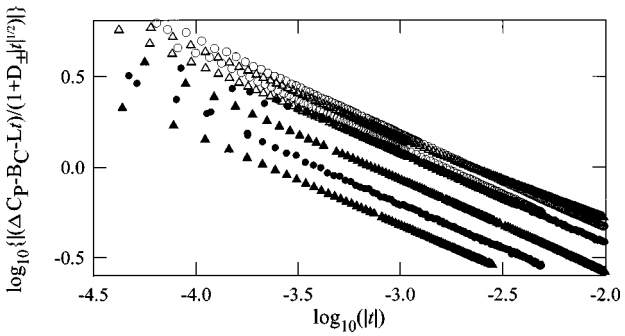

FIG. 13. Logarithmic plots for the Millipore confined mixtures. The slope in all cases is the same as for pure bulk 9CB. The open and closed circles correspond to the bulk and 50*M* Millipore confined 9.05CB, respectively. Open (closed) triangles represent bulk (confined) 9.11CB.

± 0.05. In the 50*M* Millipore where for pure 9CB an effective crossover exponent was obtained ($\alpha=0.36$), in the mixture cases, the tricritical behavior is recovered: $\alpha=0.5\pm 0.01$ for both 9.11CB and 9.05CB. The amplitude ratio is 2.30 ± 0.08 and 2.51 ± 0.17 for 9.05CB and 9.11CB, respectively, considerably different from the bulk mixtures. The confined amplitude ratios are consistent with what can be expected given the peak shapes. Forcing α to be the same on both sides of the transition peak and an amplitude ratio different from unity reflects the asymmetric nature of the peak. The fitting parameters are listed in Table III.

DISCUSSION AND CONCLUSIONS

From the combined results of the critical behavior analysis of bulk and confined 8CB, 9CB, and 9CB+10CB mixtures, it is clear that substantial changes are introduced by the random Millipore confinement. A near zero heat capacity exponent is obtained when the void size is below 220*M* (or 50*M*) for 8CB (or 9CB). It is well known that the critical behavior at the Sm-*A*–*N* transition is influenced by the coupling between the smectic-*A* order parameter and the nematic order parameter and director fluctuations. Depending on the strength of the coupling, proportional to the width of the nematic phase, the critical behavior falls into different regimes: 3D *XY* ($\alpha=-0.007$), crossover (a nonuniversal, effective $\alpha=0.2-0.3$), and tricritical ($\alpha=0.5$) with increased coupling strength. The bulk 8CB and 9CB belong to the nonuniversal crossover and near tricritical behavior, respectively. In Millipore, the exponent α is driven from its bulk value towards the 3D-*XY* value with decreasing void size (or, increased confinement) for both 8CB and 9CB. The size at which this occurs is smaller for the narrower nematic range material. When liquid-crystal mixtures were studied, thereby increasing the order parameter coupling, the confinement did not affect the critical exponent. See Fig. 14.

This confinement-induced α behavior with decreasing void size is analogous to results for bulk (7+8)CB mixtures [11] as a function of (smecticless) 7CB concentration. In the (7+8)CB mixture system, a significant decrease of the exponent α was observed with increasing 7CB concentration. Larger amounts of 7CB increased the nematic range and thus weakened the coupling between order parameters. Conse-

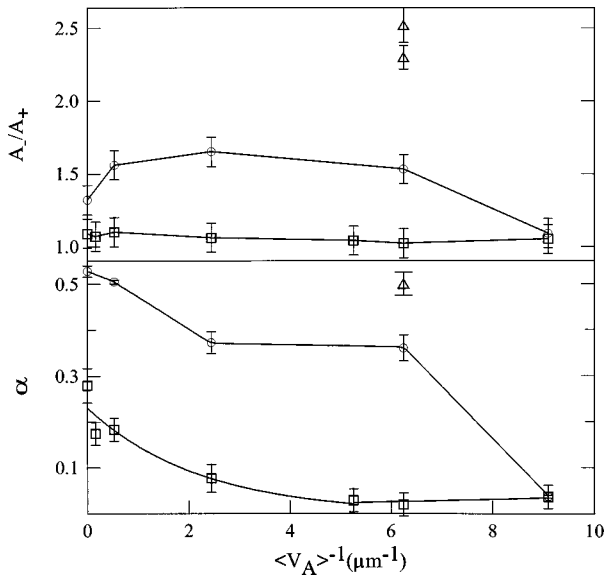

FIG. 14. Critical exponent α and amplitude ratio A_+/A_- dependence on the Millipore average void size for 8CB (□) and 9CB (○). (△) represents the mixture results. Solid lines are guides to the eye.

quently, the random confinement drives the Sm-$A-N$ transition towards the 3D-XY universality class.

One can speculate on a possible mechanism through which the confinement might be able to alter the coupling between order parameters that might be termed a ''truncation model.'' Under random confinement, director fluctuations are truncated at length scales where the correlation length is comparable to the void size R. Since a bound (pinned) surface layer of liquid crystal (LC) exists on the fiber surface, the strength of these fluctuations decreases for wavelengths approaching R. Long wavelength fluctuations, such as director fluctuations and spatial fluctuations of the smectic layers, are suppressed; shorter wavelengths such as order parameter fluctuations are also restricted but to a lesser extent. This mechanism should be reflected in longer relaxation times for correlations as observed in quasielastic light scattering studies for 8CB in Aerogel [1,20]. However, sharp transitions are not present in any pore size Aerogel, an equally randomly interconnected porous medium.

Below a liquid-crystal material dependent ''critical'' dimension R_C, the smectic order parameter is effectively decoupled from the nematic order parameter. In Millipore, the ratio of the R_C's of 8CB to 9CB is $0.22/0.05=4.4$ as determined by the nominal size, or, $3.24/1.15=2.8$ if one uses the x-ray scattering results for the saturated correlation length. The average value of these results, 3.6, is tantalizingly close to the ratio of their nematic ranges ($7.1/1.9=3.7$). The efficiency of the decoupling mechanism is evidently dependent on the bulk universality and the void size. For instance, 0.05 μm Millipore drives 8CB's nonuniversal crossover ($\alpha=0.28$) critical behavior to 3D-XY behavior, 9CB's tricritical behavior ($\alpha=0.5$) to nonuniversal ($\alpha=0.36$) behavior; but leaves the tricritical behavior in 9.05CB and 9.11CB unaffected. These observations are in agreement with those in Aerosil where, for instance, the critical behavior is unaffected by the confinement when the bulk liquid crystal already belongs to the 3D-XY criticality [16].

The Sm-$A-N$ transition peak width and transition enthalpy, FWHM, and $\Delta H_{\text{Sm-}A-N}$, also suggest a critical dimension. For 8CB, a drastic change in both FWHM and $\Delta H_{\text{Sm-}A-N}$ (see Table II, inset to Fig. 4, and Fig. 5) takes place below the 220M sample void size. For 9CB, the critical void size is below that of the 50M sample. The ''critical'' dimensions obtained from the peak width and shape analysis, not related to the critical behavior, are consistent with the ''critical'' dimensions that were obtained from the critical behavior analysis.

To conclude, we have provided experimental evidence that the interconnected Millipore confinement introduces random fields that substantially affect the specific heat critical behavior. In particular, the random confinement drives the Sm-$A-N$ transition towards 3D-XY criticality. It would be extremely illuminating to study such a confined-induced crossover in other critical quantities.

ACKNOWLEDGMENTS

We are grateful to Professor Noel Clark and his group for performing and providing us with the synchrotron scattering results, and Professor Paul Sokol for collaborating with us in the SANS measurements. This work was supported by NSF-STC ALCOM Grant No. DMR 89-20147.

[1] N. A. Clark, T. Bellini, R. M. Malzbender, B. N. Thomas, A. G. Rappaport, C. D. Muzny, D. W. Schaefer, and L. Hrubesh, Phys. Rev. Lett. **71**, 3505 (1993); L. Wu, B. Zhou, and C. W. Garland, Phys. Rev. E **51**, 2157 (1995); T. Bellini, N. Clark, and D. W. Schaefer, Phys. Rev. Lett. **74**, 2740 (1995).

[2] G. S. Iannacchione, G. P. Crawford, S. Zumer, J. W. Doane, and D. Finotello, Phys. Rev. Lett. **71**, 2595 (1993); G. S. Iannacchione, G. P. Crawford, S. Qian, J. W. Doane, S. Zumer, and D. Finotello, Phys. Rev. E **53**, 2402 (1996).

[3] G. S. Iannacchione and D. Finotello, Phys. Rev. Lett. **69**, 2094 (1992); Phys. Rev. E **50**, 4780 (1994).

[4] G. P. Crawford, D. Yang, S. Zumer, D. Finotello, and J. W. Doane, Phys. Rev. Lett. **66**, 72 (1991).

[5] S. Kralj and S. Zumer, Phys. Rev. E **54**, 1610 (1996).

[6] P. E. Cladis, Philos. Mag. **29**, 641 (1974).

[7] J. T. Mang, K. Sakamoto, and S. Kumar, Mol. Cryst. Liq. Cryst. Sci. Technol., Sect. A **222**, 133 (1992).

[8] G. S. Iannacchione, J. T. Mang, S. Kumar, and D. Finotello, Phys. Rev. Lett. **73**, 2708 (1994).

[9] C. W. Garland and G. Nounesis, Phys. Rev. E **49**, 2964 (1994); and references therein.

[10] W. L. McMillan, Phys. Rev. A **7**, 1419 (1973).

[11] J. Thoen, H. Marynissen, and W. Van Dael, Phys. Rev. Lett. **52**, 204 (1984).

[12] G. Nounesis, C. W. Garland, and R. Shashidhar, Phys. Rev. A **43**, 1849 (1991).

[13] D. Brisbin, R. DeHoff, R. E. Lockhart, and D. L. Johnson, Phys. Rev. Lett. **43**, 1171 (1979).
[14] B. M. Ocko, R. J. Birgeneau, and J. D. Litster, J. Phys. B **62**, 487 (1986).
[15] S. Qian, G. S. Iannacchione, and D. Finotello, Phys. Rev. E **53**, R4291 (1996).
[16] B. Zhou, G. S. Iannacchione, C. W. Garland, and T. Bellini, Phys. Rev. E **55**, 2962 (1997).
[17] G. B. Kasting, C. W. Garland, and K. J. Lushington, J. Phys. (Paris) **41**, 879 (1980).
[18] I. Hatta and T. Nakayama, Mol. Cryst. Liq. Cryst. **66**, 97 (1981).
[19] J. Thoen, H. Marynissen, and W. Van Dael, Phys. Rev. A **26**, 2886 (1982).
[20] X.-I. Wu, W. I. Goldburg, M. X. Liu, and J. Z. Xue, Phys. Rev. Lett. **69**, 470 (1992).
[21] A. Zidansek, S. Kralj, G. Lahajnar, and R. Blinc, Phys. Rev. E **51**, 3332 (1995).
[22] See, for instance, several reviews in *Liquid Crystals in Complex Geometries Formed by Polymer and Porous Networks*, edited by G. P. Crawford and S. Zumer (Taylor & Francis, London, 1996).
[23] G. S. Iannacchione, S. Qian, D. Finotello, and F. M. Aliev, Phys. Rev. E **56**, 554 (1997).
[24] S. Tripathy, C. Rosenblatt, and F. M. Aliev, Phys. Rev. Lett. **72**, 2725 (1994).
[25] BDH Ltd., Poole, England.
[26] Millipore Corp., 397 Williams St., Marlborough, MA 01752.
[27] S. Qian, G. S. Iannacchione, D. Finotello, L. M. Steele, and P. E. Sokol, Mol. Cryst. Liq. Cryst. Sci. Technol., Sect. A **265**, 395 (1995).
[28] N. Clark (private communication).
[29] D. Finotello and G. S. Iannacchione, Int. J. Mod. Phys. **9**, 2247 (1995).
[30] A. G. Rappaport, N. Clark, B. N. Thomas, and T. Bellini, in *Liquid Crystals in Complex Geometries Formed by Polymer and Porous Networks*, edited by G. P. Crawford and S. Zumer (Taylor & Francis, London, 1996), Chap. 20.
[31] K. Ema, G. Nounesis, C. W. Garland, and R. Shashidhar, Phys. Rev. A **39**, 2599 (1989); X. Wen, C. W. Garland, and M. D. Wand, *ibid.* **42**, 6087 (1990); K. J. Stine and C. W. Garland, Mol. Cryst. Liq. Cryst. **188**, 91 (1990).
[32] R. M. Marroum, G. S. Iannacchione, D. Finotello, and M. A. Lee, Phys. Rev. E **51**, R2743 (1995).
[33] T. Bellini, C. Chiccoli, P. Pasini, and C. Zannoni, Phys. Rev. E **54**, 2647 (1996).
[34] H. Lin, P. Palffy-Muhoray, and M. A. Lee, Mol. Cryst. Liq. Cryst. **204**, 189 (1991).
[35] P. Sheng, Phys. Rev. Lett. **37**, 1059 (1976); Phys. Rev. A **26**, 1610 (1982).
[36] Our NMR measurements in Millipore show that surface-induced ordering exists in the isotropic phase. This surface-induced ordering is weaker than in any other porous material that we have studied.
[37] A. Aharony and M. E. Fisher, Phys. Rev. B **27**, 4394 (1983).
[38] S. T. Shin, S. Kumar, D. Finotello, S. S. Keast, and M. E. Neubert, Phys. Rev. A **45**, 8683 (1992).
[39] C. Bagnuls and C. Bevillier, Phys. Rev. B **32**, 7209 (1985); see also C. Bagnuls, C. Bevillier, D. I. Meiron, and B. G. Nickel, *ibid.* **35**, 3585 (1987).
[40] W. H. Press, B. P. Flannery, S. A. Teukolsky, and W. T. Vetterling, *Numerical Recipes—The Art of Scientific Computing* (Cambridge University Press, Cambridge, England, 1989).
[41] H. Marynissen, J. Thoen, and W. Van Dael, Mol. Cryst. Liq. Cryst. **97**, 149 (1983).